Effects of Lithium Doping in TiO₂ Thin Films on Their Structural, Optical, and Morphological Properties, and on the Degradation Efficiency of Methylene Blue Dye

A. Doula^{a,*} and R. Bensaha^b

Received: 04.08.2025 & Accepted: 25.09.2025

Doi: 10.12693/APhysPolA.148.166

*e-mail: doula.a@centre-univ-mila.dz

In this study, we investigate the impact of lithium (Li⁺) doping on the structural, morphological, optical, and photocatalytic properties of TiO_2 thin films. Li⁺-doped TiO_2 films were fabricated on glass substrates using the sol–gel spin-coating technique and subsequently annealed at 550°C for 2 h. X-ray diffraction analysis confirmed that all films crystallize exclusively in the anatase phase. The crystallite size was found to decrease from 19 to 13 nm with increasing Li⁺ doping. The surface morphology, examined through scanning electron microscopy and atomic force microscopy, revealed noticeable changes influenced by the Li⁺ content. With higher Li⁺ concentrations, optical transmittance (T [%]) increased, while the optical band gap (E_g [eV]) decreased. Additionally, lithium doping enhanced the photocatalytic efficiency of TiO_2 films in degrading methylene blue.

topics: TiO₂ thin film, Li⁺ doping, spin-coating, photocatalytic activity

1. Introduction

Environmental pollution — especially water contamination — remains a critical global challenge with serious implications for human health. Among the numerous pollutants, synthetic dyes widely used in the textile industry (such as methylene blue (MB)) are of particular concern. Numerous studies have investigated physical, chemical, and biological approaches to the treatment and removal of such organic pollutants from wastewater.

Heterogeneous photocatalytic process involving semiconductors is an eco-friendly technology that has shown promise in addressing environmental pollution issues [1]. When a semiconductor is exposed to light with energy greater than its band gap, electrons are excited from the valence band to the conduction band, creating electron—hole pairs. These holes react with surface hydroxyl ions or water to produce hydroxyl radicals (${}^{\bullet}$ OH), while electrons interact with absorbed molecular oxygen to form superoxide anion radicals (${}^{\bullet}$ O $_2^-$), which help oxidize and mineralize toxic organic compounds [2].

Many semiconductor oxides, ZrO₂ [3, 4], ZnO [5], CdS [6], MoS₂, Fe₂O₃, WO₃ [7, 8], and titanium dioxide (TiO₂) included, have been identified as

effective photocatalysts [9, 10]. TiO₂, in particular, is widely studied due to its abundance, cost-effectiveness, and environmental friendliness [11]. However, its photocatalytic efficiency is limited by issues like rapid electron—hole recombination and low specific surface area [12, 13].

To enhance the ${\rm TiO_2}$'s photocatalytic performance, it is necessary to increase its surface area by reducing its grain size to the nanometer scale [14, 15]. This modification provides more active sites for pollutant adsorption and accelerates their decomposition. Additionally, introducing metallic (${\rm Li^+}$, ${\rm Zn^{2+}}$, ${\rm Cd^{2+}}$, ${\rm Ce^{3+}}$, ${\rm Mn^{2+}}$, ${\rm Fe^{3+}}$) or non-metallic (N, S, C, B, P, I, F) dopants into the ${\rm TiO_2}$ matrix can create new electronic trapping levels within the band gap [16–18], reducing the energy gap and slowing electron–hole recombination [19–21].

Studies have shown that doping TiO₂ with lithium (Li⁺) improves its photocatalytic activity in the degradation of various organic pollutants. For instance, Bouattour et al. [22] demonstrated that Li⁺-doped TiO₂ prepared via the sol–gel method outperforms undoped TiO₂ in removing five organic pollutants under solar irradiation. Ravishankar et al. [23] found that Li⁺ doping enhances the photodegradation of blue dye trypan under ultraviolet

^aScience and Technology Department, Abdelhafid Boussouf University Center of Mila, Mila, Algeria

^bPhysics Department, Fréres Mentouri University, Constantine, Algeria

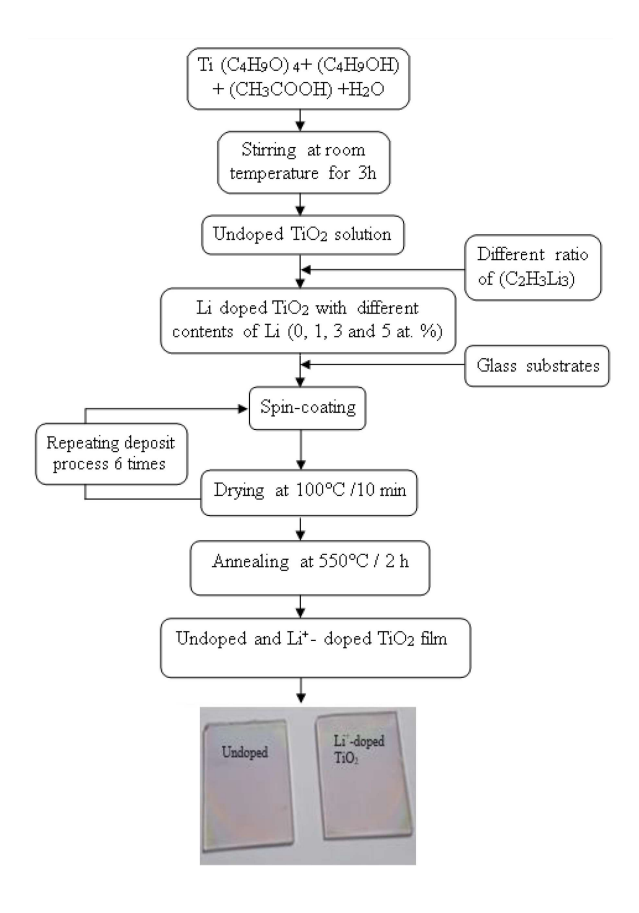


Fig. 1. Process of fabrication of undoped and ${\rm Li}^+$ -doped ${\rm TiO}_2$ thin films.

(UV) light radiation and detoxifies Cr^{+6} to nontoxic Cr^{+3} . Brezova et al. [16] observed that Li^+ -doped TiO_2 nanoparticles prepared by the sol–gel method are more efficient in the phenol removal under UV light. However, Lopez et al. [24] reported a decrease in the photocatalytic degradation of 2,4-dinitroaniline upon doping with Li^+ , and Bessekhouad et al. [25] obtained mixed results, with some TiO_2 catalysts showing reduced photoactivity and others exhibiting better performance, depending on the preparation methods and conditions.

Powder photocatalysts face two main challenges, i.e., the difficulty of separating the catalyst from water, which requires additional steps, and poor light distribution. To address these, photocatalyst films deposited on various substrates offer promising solutions [19, 26]. To date, the photocatalytic performance of Li⁺-doped TiO₂ thin films has not been extensively studied.

This study aims to examine the effect of lithium doping (0, 1, 3, and 5 at.%) on the structural, morphological, and optical properties of TiO_2 thin films synthesized via the sol–gel spin-coating technique. Additionally, we investigated how these properties influence the films' photocatalytic efficiency in the degradation of MB dyes under UV irradiation. The findings indicate that low concentrations of Li^+

doping lead to a reduction in both the grain size and the band gap energy of the anatase-phase of TiO₂, thereby significantly enhancing its photocatalytic activity in wastewater treatment.

2. Experimental details

2.1. Films preparation

Thin layers of undoped and Li⁺-doped TiO₂ were deposited on glass substrates using the solgel spin-coating method. TiO₂ solution was prepared from a mixture of: 1 mol butanol (C₄H₉OH) as solvent, 4 mol acetic acid (CH₃COOH) solution as catalyst, 1 mol of distilled water, and 1 mol tetrabutyl-orthotitanate $Ti(C_4H_9O)_4$ as source of titanium [27, 28]. This mixture was stirred moderately for 3 h. Then, Li⁺-doped TiO₂ solutions with different contents of Li (0, 1, 3, and 5 at.%) were obtained by adding different ratios of lithium acetate $(C_2H_3Li_3)$ to TiO_2 solution. These solutions were stirred for 6 h at room temperature and spin-coated, onto glass substrates at 3000 rpm for 30 s as speed of rotation. After each coating, the samples were dried at 100°C for 10 min. This coating and heating process was repeated 6 times. Finally, the samples were annealed at 550°C for 2 h. Figure 1 shows the fabrication process of undoped and Li^+ -doped TiO_2 thin films.

2.2. Films characterization

The structural properties were characterized using a Panalytical Empyrean X-ray diffractometer (XRD) in grazing incidence mode with Cu K_{α} radiation ($\lambda_{\text{Cu}K_{\alpha}}=1.54056$ Å). Optical transmission was performed by a JASCO UV-visible spectrophotometer. Film surface morphology was observed using an Asylum Research (MFP-3D SPM) atomic force microscope (AFM) and a TESCAN VEGA TS 5130 MM type scanning electron microscope (SEM). Energy-dispersive X-ray (EDX) spectroscopy measurements were performed on a 5 at.% Li⁺-doped TiO₂ film for elemental analysis.

2.3. Photodegradation tests

Methylene blue (MB) solution (volume: 25 ml, concentration: 10^{-5} mol/l) were used as models for organic pollutants to study the effect of lithium doping on the photocatalytic efficiency of TiO₂ thin films under ultraviolet light source (model VL-215.LC, maximum power 15 W, wavelength $\lambda = 365$ nm) for 210 min. Every 30 min, 4 ml of MB solutions were extracted and analyzed by UV spectroscopy (JASCO).

3. Results and discussion

3.1. Structural properties

Figure 2 shows the X-ray patterns of ${\rm TiO_2}$ thin films (undoped and doped with various ${\rm Li^+}$ contents) annealed at 550°C for 2 h. As one can see, Fig. 2 illustrates the presence of peaks corresponding to the (101), (004), (200), (105), and (211) planes of the anatase phase (JCPDS 21-1272). Furthermore, the intensity of all diffraction peaks decrease as a function of ${\rm Li^+}$ doping, indicating a decreases in the crystallinity of the film. In addition, no lithium oxide-related peaks were found in any of diagrams, which may be attributed to the low ${\rm Li^+}$ doping content.

Additionally, the crystallite size (L) of undoped and Li⁺-doped TiO₂ thin films can be deduced from the XRD broadening peak of (101) using the Scherrer equation [29]. Therefore,

$$L = \frac{0.94\lambda}{\beta\cos(\theta)},\tag{1}$$

where L is the crystallite size in nm, λ is the wavelength of X-ray ($\lambda_{\text{Cu}K_{\alpha}} = 1.54056 \text{ Å}$), β is the full width at half maximum (FWHM) of the (101) diffraction peak, and θ is the Bragg angle in radian.

In addition, the dislocation density (δ) and microstrain (ε) in the films has been determined using the following formulas [30], respectively,

$$\delta = \frac{1}{L^2} \tag{2}$$

and

$$\varepsilon = \frac{\beta \cos(\theta)}{4}.\tag{3}$$

These parameters are important for our analysis. Microstrain describes minor, irregular distortions in the crystal lattice caused by the defects such as dislocations or vacancies. The goal of calculating δ is to identify defects in the crystal lattice and understand the resulting structure of the lattice crystal. An increase in δ leads to an increase in lattice defects, and thus a decrease in the crystallinity and grain size of the films. On the other hand, stress, as another known parameter, refers to the internal force exerted per unit area within a material.

TABLE I Structural parameters obtained from XRD patterns of undoped and ${\rm Li}^+$ -doped TiO₂ thin films.

Samples	L [nm]	$\frac{\delta \times 10^{14}}{[\text{lines/m}^2]}$	$\varepsilon \times 10^{-2}$	
Undoped	19	29.20	11.46	
$1~{\rm at.\%}$	18	31.48	12.17	
3 at. %	17	35.95	12.67	
$5~\mathrm{at.\%}$	13	62.14	16.56	

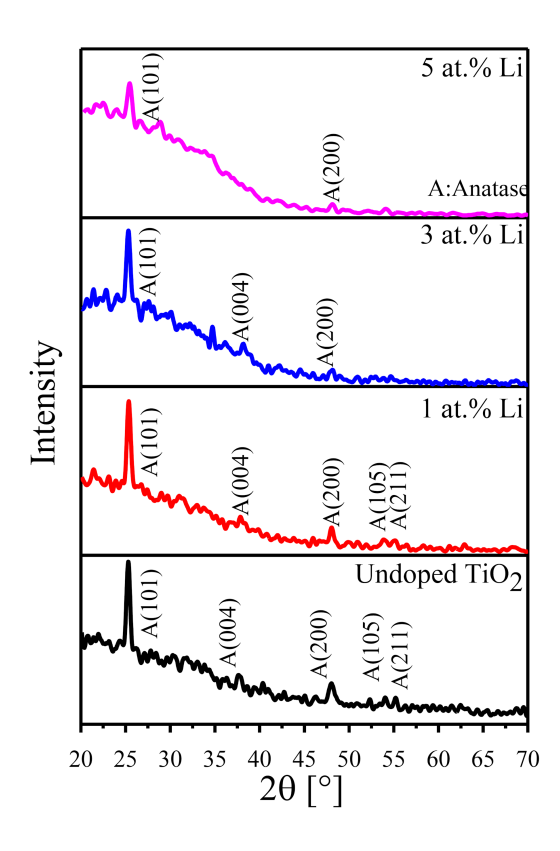


Fig. 2. XRD patterns of undoped and various Li⁺-doped TiO₂ thin films annealed at 550°C.

As presented in Table I, increasing the Li⁺ content led to a reduction in crystallite size, suggesting a decline in the crystallinity of the films. This decrease can be attributed to the substitution of ${\rm Ti}^{4+}$ ions by Li⁺ ions within the TiO₂ lattice. Since the ionic radius of Li⁺ (0.99 Å) is larger than that of ${\rm Ti}^{4+}$ (0.68 Å), the incorporation of Li⁺ induces internal lattice stress, thereby hindering the growth of TiO₂ crystallites. Furthermore, Table I also indicates that both the dissociation intensity and internal microstrain within the films increase with higher Li⁺ concentrations, which may further contribute to the degradation of the crystalline structure [31].

3.2. Optical properties

Figure 3 shows the optical transmittance spectra of undoped ${\rm TiO_2}$ and ${\rm TiO_2}$ thin films doped with various concentration of ${\rm Li^+}$. These spectra were used to estimate the films thicknesses using the envelope method [32]. Table II lists the corresponding values. As a result, the thicknesses were found not to be significantly affected by the lithium content.

Figure 3 also shows that all films have high transmittance of about 85% in the visible region. Likewise, the presence of interference fringes in this region is attributed to interference effect, indicating that the films studied are sufficiently thick.

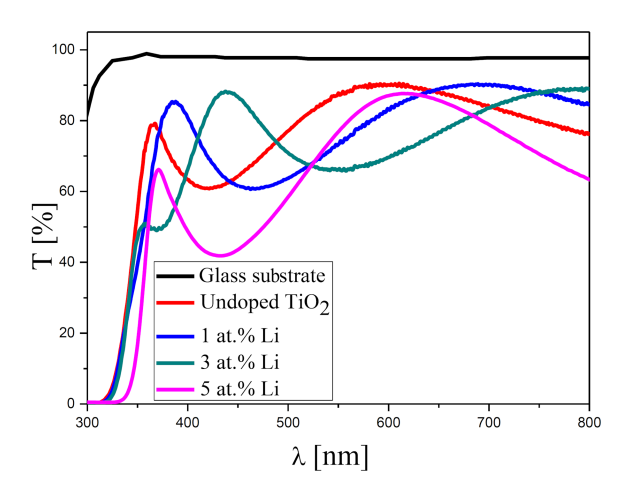


Fig. 3. Transmission spectra T [%] of undoped and Li^+ -doped TiO_2 thin films.

TABLE II

Gap energy (E_g) , thicknesses and roughness mean square (RMS) of surface of Li⁺-doped TiO₂ thin films.

Samples	Thicknesses [nm]	E_g [eV]	RMS [nm]
$\operatorname{Undoped}$	142	3.45	1.35
$1~{\rm at.\%}$	141	3.40	2.98
$3~{\rm at.\%}$	142	3.37	0.95
$5~\mathrm{at.\%}$	143	3.32	1.26

Beside, all thin films begin to absorb light close to the UV region. As the ${\rm Li}^+$ concentration increases, the absorption edge shifts towards longer wavelengths. This shift may be correlated to a decrease in the optical band gap energy (E_g) . This, in fact, can be deduced by applying Tauc's formula [33]

$$(\alpha h \nu)^2 = A \left(E_q - h \nu \right), \tag{4}$$

where A is a constant, $h\nu$ is the photon energy, E_g is the optical band gap, and α is the absorption coefficient.

Figure 4 displays the deduction of the optical band gap (E_q) of the studied films in the form of a curve intersected with the abscissa axis, assuming the relation as $(\alpha h \nu)^2 = f(h \nu)$ [34, 35]. Table II summarizes the corresponding values of E_g [eV]. The band gap of the thin film decreases from 3.45 to 3.32 eV, depending on the Li⁺ doping. The diminishing of E_g related to the insertion of Li⁺ doping may be attributed to the formation of new energy levels in the TiO₂ band gap [36, 37]. From an energy point of view, the decrease in the band gap permits the absorption of more energy which, on the one hand, increases the concentration of electron-hole pairs. On the other hands, it effectively improves the photocatalytic activity [38].

3.3. Surface morphology

3.3.1. Scanning electron microscopy (SEM) analyze

Figure 5 illustrates the surface morphology of (a) undoped TiO₂, (b) 1 at.% Li⁺-doped TiO₂, and (c) 5 at.% Li⁺-doped TiO₂, annealed at 550°C for 2 h. As we can observe, all films characterized by granular nanostructure are relatively homogeneously distributed on the surface, without forming agglomerations. On the other hand, as the Li⁺ content increases, the particles size decreases, demonstrating that doping the TiO₂ thin films with Li⁺ inhibits the growth of TiO₂ particles. Similar results were observed by Y. Guo et al. [39]. It is worth noting that this result is in a good agreement with our XRD results. Moreover, the observed defects in the form of pores and holes along the surface of the films increase with increasing Li⁺ content. This leads to a large specific surface area, which enhances the photocatalytic activity of TiO₂ thin films [40].

It is important to mention that SEM imaging performed on TiO₂ films was very challenging because of the films' low electrical conductivity, which induces a charging effect. (So, SEM pictures appeared too hazy.)

The elemental chemical composition of the 5% Li⁺-doped TiO₂ film was identified by the energy-dispersive X-ray (EDX) spectrum, as shown in Fig. 5d. The Ti and O peaks can be clearly detected. Beside the presence of the substrate components (Si and Ca), the element Au is also detected, which is due to the metallization. No Li⁺ peaks have been detected because lithium has low atomic number (Z=3), which means that it is one of the elements difficult to detect by EDX analysis (elements with atomic number below 11 are very difficult to detect [41]). Comparable results were recorded by Ajala et al. [42]. The authors reported that lithium was not detected by EDX spectroscopy in the case of 10% Li⁺-doped ZnO films prepared by the sol-gel method.

3.3.2. Atomic force microscopy (AFM) analyze

Figure 6 presents results from atomic force microscopy (AFM) for undoped and Li⁺-doped TiO₂ thin films annealed at 550°C during 2 h. The AFM images show a homogeneous granular surface morphology. In addition, a decrease in the mean grain size and the emergence of cracks are observed at the sites scattered on the surface upon increasing the Li⁺ content. The roughness mean square (RMS) of the film thickness changes between 0.95 and 2.98 nm depending on the Li⁺ doping. This result may be related to the variation in the surface morphology and the appearance of pores and cracks.

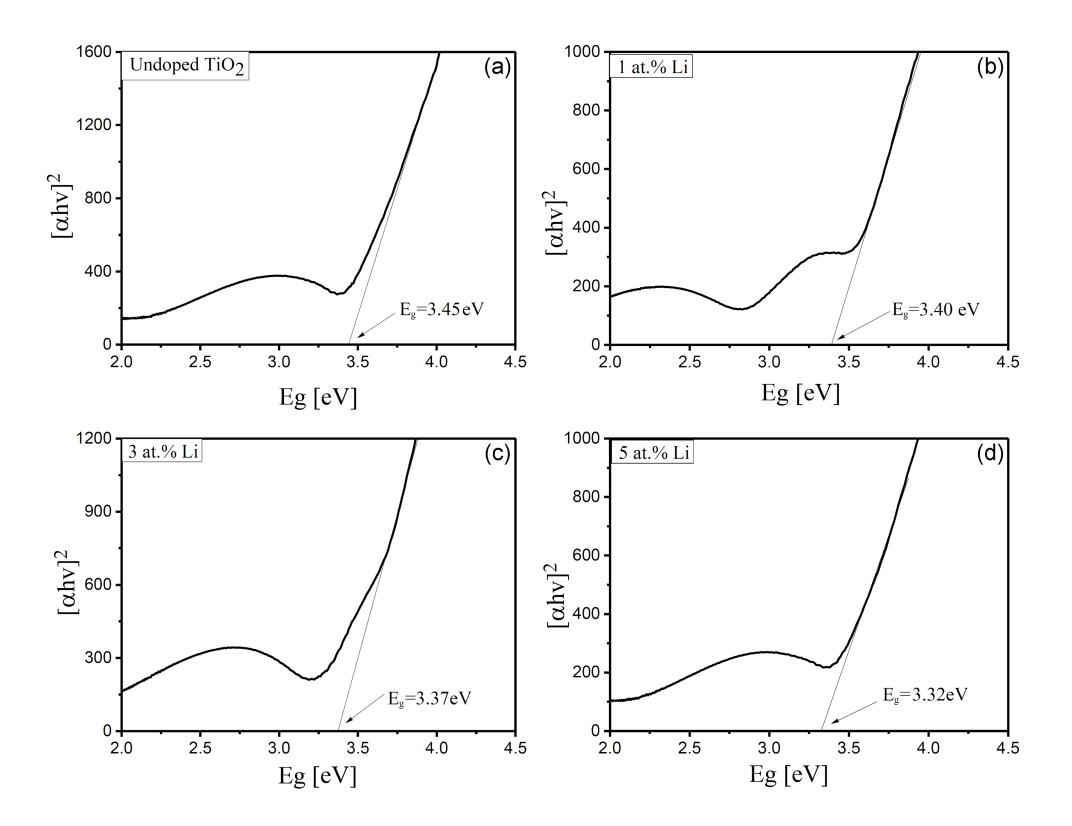


Fig. 4. The plots of $(\alpha h\nu)^2$ versus photon energy $(E_g = h\nu)$ of TiO₂ thin films: (a) undoped and (b-d) doped with Li⁺.

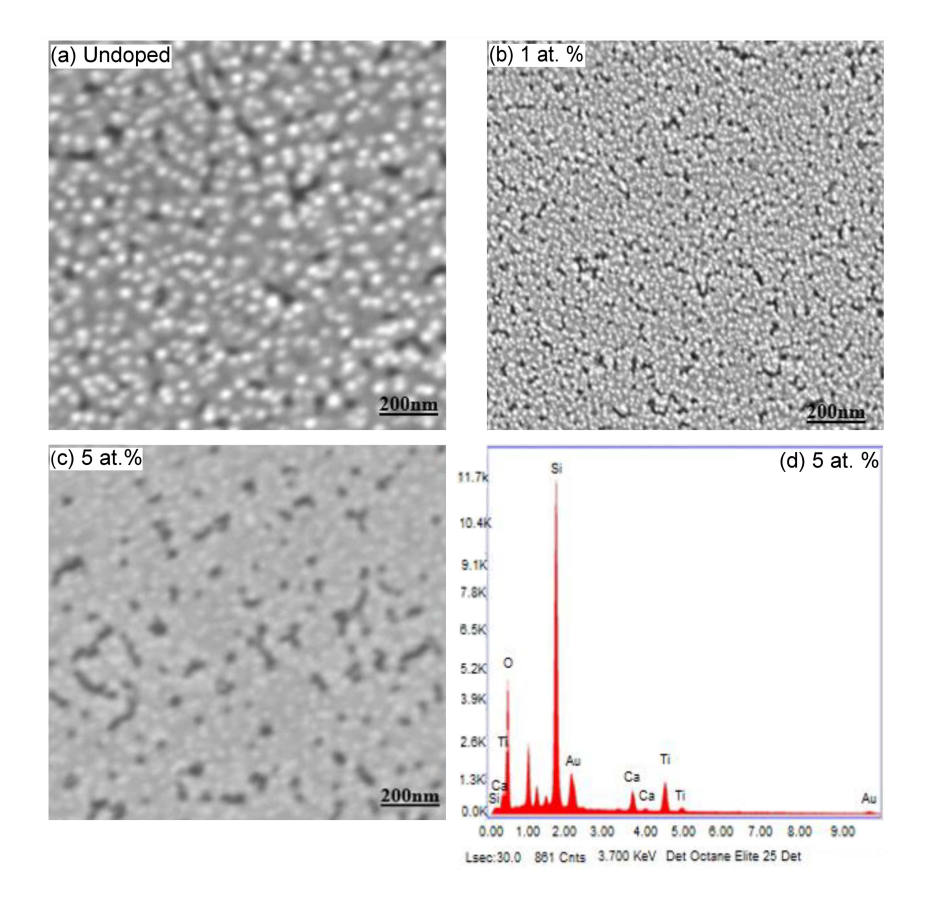


Fig. 5. SEM micrographs of (a) undoped and (b–c) Li^+ -doped TiO_2 thin films and (d) EDX spectrum of TiO_2 film doped with 5 at.% of Li.

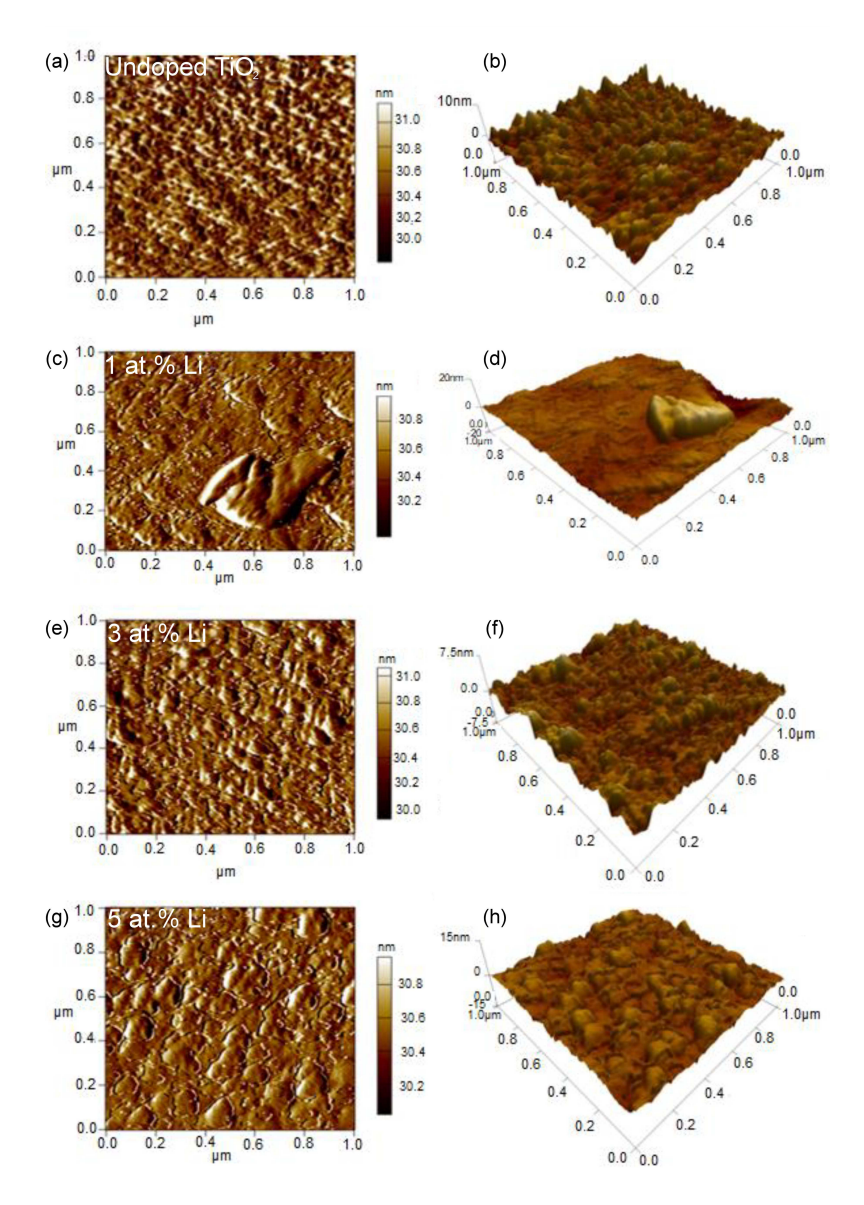


Fig. 6. (a, c, e, g) 2D and (b, d, f, h) 3D AFM micrographs of TiO₂ thin films with different Li⁺¹ content.

3.4. Photocatalytic properties

The degradation of the methylene blue (MB) solution under UV irradiation for 210 min was studied to assess the impact of ${\rm Li}^+$ doping on the photocatalytic performance of ${\rm TiO_2}$ thin films. Figure 7 presents the MB absorption spectra recorded at various UV-exposure times, using ${\rm TiO_2}$ thin films doped with 5 at.% of ${\rm Li}^+$ as the photocatalyst. A gradual decrease in the absorption peak at 654 nm is observed with increasing irradiation time. The photodegradation efficiency D [%] was determined using [43]

$$D = \frac{(C_0 - C)}{C_0} \times 100,\tag{5}$$

where C_0 is the initial concentration, and C is the concentration at a given time.

Figure 8 illustrates the photodegradation rate $(D \ [\%])$ of MB solutions. After exposing the solution without photocatalyst to UV irradiation for 210 min, the degradation of MB was negligible. However, the inclusion of the TiO₂ photocatalysts (either undoped or Li⁺-doped) significantly enhanced the photodegradation rate D, which increased with higher Li⁺ content. This trend suggests a notable improvement in photocatalytic activity. Notably, TiO₂ films doped with 5 at.% of Li⁺ exhibited the highest performance (92%). Furthermore, the photocatalytic degradation follows a pseudo-first-order reaction, and therefore the rate constant (K) can be determined using [44]

$$\ln\left(\frac{C_0}{C}\right) = Kt,$$
(6)

where K [min⁻¹] is the apparent rate constant, and t [m] is the irradiation time.

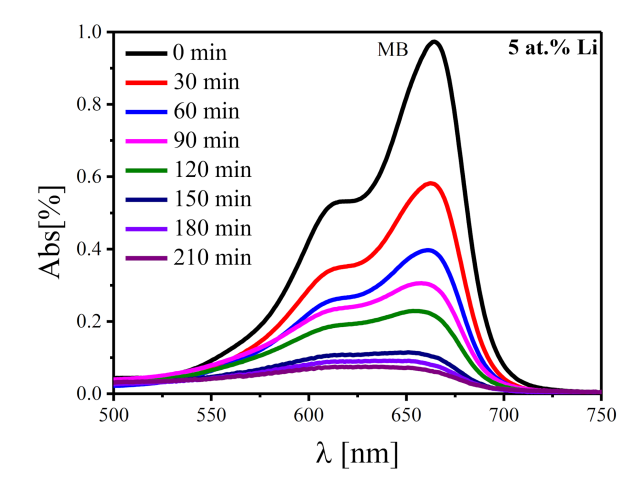


Fig. 7. Absorption spectra of MB obtained at different UV-irradiation times using the 5 at.% Li⁺-doped TiO₂ thin film.

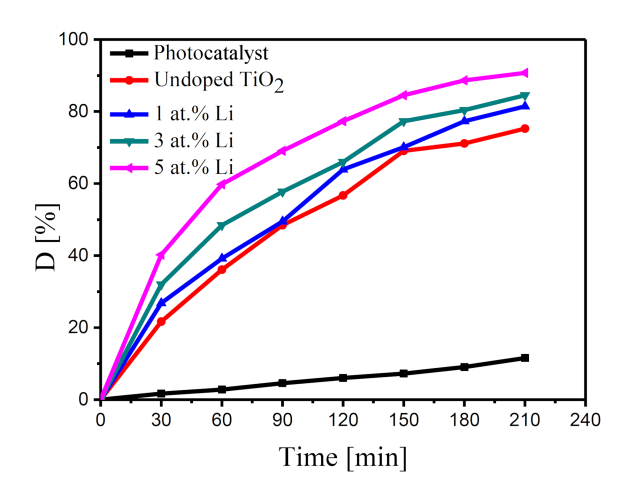


Fig. 8. Photodegradation rate of MB using undoped and Li⁺-doped TiO₂ thin films.

Figure 9 shows a plot of $\ln(C_0/C)$ versus irradiation time t. The values of the rate constant K are obtained by the slope of each curve. As the lithium content increases, the K value increases. This indicates that the insertion of lithium improves the photocatalytic activity of TiO_2 . Thus, the 5% Li⁺-doped TiO_2 film exhibits the fastest performance in decomposing MB in water.

The increase in photocatalytic activity of TiO₂ films as a function of lithium content can be related to the following factors:

- (i) The decrease in grain size (see Table I) leads to an increase in the surface area and thus provides more active sites for reactive molecules, which improves the electron-hole separation rate [45].
- (ii) The decrease in the band gap (see Table II) allows for the absorption of more energy, leading to greater production of electron—hole pairs [19, 46]. As a result, more electrons

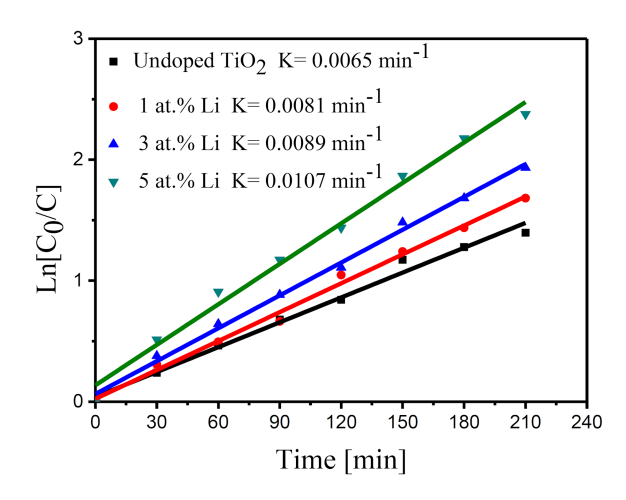


Fig. 9. The plot of $\ln(C_0/C)$ versus time showing the degradation rate constant (K) of MB.

- and holes can contribute in the photoreaction and thus enhance the removal of organic molecules.
- (iii) Li⁺ doping forms an energy level in the band gap of TiO₂ and improves the electron-hole separation rate [19, 47]. Consequently, the ability of Li ions to act as electron traps reduces recombination of the electron-hole pair. This behavior causes the photogenerated holes to be available for reaction with hydroxyl ions present in water to form OH⁻ radicals [22, 47].
- (iv) From SEM analysis, it appears that the 5 at.% Li⁺-doped TiO₂ film shows (see Fig. 5) a higher number of pores, which provides more active sites for adsorption of pollutant molecules. Also, it improves the effectiveness of the photocatalyst [48].

As for other literature works on the removal of MB from water using metal-doped ${\rm TiO_2}$ thin films, Xiaodong Zhuet al. [49] evaluated the removal of MB dye using Nd:TiO₂ films. They have found that the films achieved a degradation rate around 25.9% after 4 h of UV light irradiation. Furthermore, Bensouici et al. [50] reported that Cu:TiO₂ thin films displayed a degradation rate of 16% after 180 min of the removal of MB under UV light irradiation.

4. Conclusions

In this study, we focused on examining the influence of varying lithium concentrations $(0,\,1,\,3,\,$ and 5 at.%) on the structural, morphological, and optical properties of ${\rm TiO_2}$ thin films synthesized via the sol–gel spin-coating technique. XRD analysis revealed that all films crystallized in the pure anatase phase. Increasing lithium content led to a reduction in both crystallinity and grain size. SEM and AFM

observations confirmed that ${\rm Li}^+$ doping alters the morphology of ${\rm TiO_2}$ nanoparticles. UV-visible analysis showed a decrease in the optical band gap with increasing lithium concentration, which was accompanied by enhanced photocatalytic activity. Among the samples, the ${\rm TiO_2}$ film doped with 5 at.% of ${\rm Li}^+$ demonstrated the highest photocatalytic performance for MB degradation.

References

- [1] M. Isleyen, E.S. Ilkme, G.S.P Soylu, *Korean J. Chem. Eng.* **34**, 1786 (2017).
- [2] Y.-F. Tu, S.-Y. Huang, J.-P. Sang, X.-W. Zou, J. Alloys. Compd. 482, 382 (2009).
- [3] B.K. Moon, J.H. Jeong, S.-S. Yi, S.E. Choi, P.S. Kim, H. Choi, J.H. Kim, *J. Lumin*. 122, 873 (2007).
- [4] J. Qiu, S. Zhang, H. Zhao, Sens. Actuators B 160, 875 (2011).
- [5] O. Seven, B. Dindar, S. Aydemir, D. Metin, M.A. Ozinel, S. Icli, J. Photochem. Photobiol. A Chem. 165, 103 (2004).
- [6] A.H. Zyoud, N. Zaatar, I. Saadeddin, C. Ali, D. Parkc, G. Campet, H.S. Hilal, J. Hazard. Mater. 173, 318 (2010).
- [7] A. Fujishima, X. Zhang, D.A. Tryk, Surf. Sci. Rep. 63, 515 (2008).
- [8] U.I. Gaya, A.H. Abdullah, J. Photochem. Photobiol. C 9, 1 (2008).
- [9] K. Hashimoto, H. Irie, A. Fujishima, Appl. Phys. 44, 8269 (2005).
- [10] J.-M. Herrmann, *Top. Catal.* **34**, 49 (2005).
- [11] D.S.C. Halin, K.A. Razak, A. Azani, M.M.A.B. Abdullah, M.A.A.M. Salleh, N. Mahmed, M.M. Ramli, A.W. Azhari, V. Chobpattana, L. Kaczmarek, Acta Phys. Pol. A 138, 159 (2020).
- [12] G. Zeng, K.K. Li, H.G. Yang, Y.H. Zhang, Vib. Spectrosc. 68, 279 (2013).
- [13] Y.F. Tu, S.Y. Huang, J.P. Sang, X.W. Zou, J. Alloys. Compd. 482, 382 (2009).
- [14] W. Choi, Catal. Surv. Asia 10, 16 (2006).
- [15] M. Fernández-García, A. Martínez-Arias, J.C. Hanson, J.A. Rodriguez, J. Chem. Rev. 104, 4063 (2004).
- [16] V. Brezová, A. Blažková, L. Karpinský, J. Grošková, B. Havlínová, V. Jorík, M. Čeppan, J. Photochem. Photobiol. A Chem. 109, 177 (1997).
- [17] S.U.M. Khan, M. Al-Shahry, W.B. Ingler Jr., Science 297, 2243 (2002).
- [18] J.G. Jia, T. Ohno, M. Matsumura, *Chem. Lett.* **29**, 908 (2000).

- [19] O. Beldjebli, R. Bensaha, Y.S. Ocak, L. Amirache, R. Boukherroub, *Mater. Res. Express* 6, 085036 (2019).
- [20] Y.-F. Tu, S.-Y. Huang, J.-P. Sang, X.-W. Zou, J. Alloys. Compd. 482, 382 (2009).
- [21] H.-J. Lin, T.-S. Yang, C.-S. Hsi, M.-C. Wang, K.-C. Lee, *Ceram. Int.* **40**, 10633 (2014).
- [22] S. Bouattour, W. Kallel, A.M. Botelho do Rego, L.F. Vieira Ferreira, I. Ferreira Machado, S. Boufi, Appl. Organometal. Chem. 24, 692 (2010).
- [23] T.N. Ravishankar, G. Nagaraju J. Dupont, *Mater. Res. Bull.* **78**, 103 (2016).
- [24] T. López, J. Hernandez-Ventura, R. Gómez, F. Tzompantzi, E. Sánchez, X. Bokhimi, A. García, J. Mol. Catal. A Chem. 167, 101 (2001).
- [25] Y. Bessekhouad, D. Robert, J.-V. Weber, N. Chaoui, J. Photochem. Photobiol. A Chem. 167, 49 (2004).
- [26] J.A.B. Pérez, M. Courel, M. Pal, F.P. Delgado, N.R. Mathews, *Ceram. Int.* 43, 15777 (2017).
- [27] H. Bensouyad, H. Sedrati, H. Dehdouh, M. Brahimi, F. Abbas, H. Akkari, R. Bensaha, *Thin Solid Films* 519, 96 (2010).
- [28] R. Mechiakh, F. Meriche, R. Kremer, R. Bensaha, B. Boudine, A. Boudrioua, Opt. Mater. 30, 645 (2007).
- [29] L. Alexander, H.P. Klug, J. Appl. Phys. 21, 137 (1950).
- [30] K. Mageshwari, R. Sathyamoorthy, J. Mater. Sci. Semicon. Proc. 16, 337 (2013).
- [31] A. Doula, R. Bensaha, O. Beldjebli, *Acta Phys. Pol. A* **140**, 421 (2021).
- [32] J. Yu, G. Wang, B. Cheng, M. Zhou, *Appl. Catal. B Environ.* **69**, 171 (2007).
- [33] M. Sreemany, S. Sen, *Mater. Chem. Phys.* 83, 169 (2004).
- [34] L. Mai, C. Huang, D. Wang, Z. Zhang, Y. Wang, *Appl. Surf. Sci.* **255**, 9285 (2009).
- [35] S. Mahanty, S. Roy, S. Sen, *J. Crystal. Growth* **261**, 77 (2004).
- [36] J. Yu, Q. Xiang, M. Zhou, *Appl. Catal. B Environ.* **90**, 595 (2009).
- [37] H. Yamashita, M. Harada, J. Misaka, M. Takeuchi, K. Ikeue, M. Anpo, J. Photochem. Photobiol. A 148, 257 (2002).
- [38] M.S. Hassan, T. Amna, O.B. Yang, H.C. Kim, M.S. Khil, *Ceram. Int.* **38**, 5925 (2012).

- [39] Y. Guo, J. Chen, Z. Ding, T.Guo, J. Wei, X. Ye, W. Xu, Z. Zhoua, RSC Adv. 6, 101714 (2016).
- [40] A. Aouina, F. Bensouici, M. Bououdina, R. Tala-Ighil, M. Toubane, F. Kezzoula, K. Chebout, *Mater. Res. Express* 6, 016406 (2019).
- [41] F. Bensouici, M. Bououdina, A.A. Dakhel, T. Souier, R. Tala-Ighil, M. Toubane, A. Iratni, S. Liu, W. Ca, *Thin Solid Film* 616, 655 (2016).
- [42] F. Ajala, H. Lachheb, N. Bouazizi, A. Houas, J. Mater Sci Mater. Electron. 28, 2817 (2017).
- [43] B.K. Kaleji, R. Sarraf-Mamoory, *Mater. Res. Bull.* 47, 362 (2012).
- [44] N.R. Mathews, E.R. Morales, M.A. Cortes-Jacome, J.A. Toledo Antonio Sol. Energy 83, 1499 (2009).

- [45] A. Arunachalam, S. Dhanapandian, C. Manoharan, *Physica E* **76**, 35 (2016).
- [46] H.-J. Lin, T.-S. Yang, M.-C. Wang, C.-S. His, J. Alloys. Compd. 610, 478 (2014).
- [47] H.-X. Li, R.-H. Xia, Z.-W. Jiang, S.-S. Chen, D.-Z. Chen, *Chin. J. Chem.* 26, 1787 (2008).
- [48] E. Cerro-Prada, M. Manso, V. Torres, J. Soriano, Front. Struct. Civ. Eng. 10, 89 (2016).
- [49] X. Zhu, H. Song, W. Feng, G. Wen, H. Li, J. Zhou, J. Adv. Oxid. Technol. 20, 20160190 (2017).
- [50] F. Bensouici, M. Bououdina, A.A. Dakhel, R. Tala-Ighil, M. Tounane, A. Iratni, T. Souier, S. Liu, W. Cai, Appl. Surf. Sci. 395, 110 (2017).